

# SPLINE INTERPOLATION IN MEDICAL IMAGING: COMPARISON WITH OTHER CONVOLUTION-BASED APPROACHES

*Erik H. W. Meijering*

Image Sciences Institute, University Medical Center Utrecht,  
NL-3584 CX, Utrecht, THE NETHERLANDS  
Tel: +31 30 250 8353; Fax: +31 30 251 3399  
E-mail: erik@isi.uu.nl

## ABSTRACT

Interpolation is required in a variety of medical image processing applications. Although many interpolation techniques are known from the literature, evaluations of these techniques for the specific task of applying geometrical transformations to medical images are still lacking. In this paper we present such an evaluation. We consider convolution-based interpolation methods and rigid transformations. The evaluation involves a large number of sinc-approximating kernels, including piecewise polynomial and windowed sinc kernels, and images from a wide variety of medical image modalities. The results show that for all modalities, spline interpolation constitutes the best trade-off between accuracy and computational cost, and therefore is to be preferred over all other methods.

## 1 INTRODUCTION

Interpolation of sampled data is required in many digital image processing operations, such as subpixel translation, rotation, elastic deformation or warping, magnification, or minification, which need to be carried out for the purpose of image registration or volume visualization. In most applications, it is of paramount importance to limit as much as possible the grey-value errors introduced by interpolation. For example, in multimodality registration of computed tomography (CT), magnetic resonance imaging (MRI), or positron emission tomography (PET) data, it has been observed that interpolation errors influence the value of the optimization cost function, which may lead to registration errors [1]. Similar problems had been reported earlier in monomodality registration of MRI images [2]. It has been pointed out that in digital subtraction angiography (DSA), improved registration and resampling methods result in improved image quality [3], which allows for reduction of contrast material or X-ray dose. It has also been pointed out [4] that in functional magnetic resonance imaging (fMRI), interpolation errors may influence the interpretation of longitudinal studies.

The common denominator in all of these applications is geometrical transformation of medical image data. Although many interpolation techniques have been put forward over the years, evaluations of these techniques for this specific task are still lacking. Recently, Ostuni *et al.* [4] compared the performance of several convolution-based interpolation techniques for the purpose of geometrical transformation. However, their study was limited to fMRI images. More elaborate evaluation studies were recently published by Lehmann *et al.* [5] and Grevera & Udupa [6]. The former study concerned geometrical transformation of medical images. However, only MRI and dental X-ray images were considered. The latter study involved a number of convolution- and shape-based interpolation methods for the purpose of slice doubling in MRI and CT images. However, the effects of these techniques on the geometrical transformation of images from these and other medical image modalities were not investigated. Moreover, we claim that the evaluation strategies used in both of these studies suffer from a number of serious shortcomings, which limit the validity of the conclusions that were drawn from them (we will return to this in Section 6).

The purpose of the present paper is to present the results of an elaborate evaluation, in which we quantitatively studied the performance of a large number of interpolation methods when using them to apply geometrical transformations to images from a wide variety of medical imaging modalities. In order to limit the size of this work, only rigid transformations were considered, in particular rotations and translations. Furthermore, the study was limited to convolution-based interpolation techniques. Although recent developments have resulted in new interpolation techniques, such as shape- or morphology-based methods [7, 8], or Fourier-based methods [9, 10], the vast majority of interpolation techniques used in medical image transformation are convolution-based techniques—probably because they are less complex than shape-based techniques (easier to implement; no or considerably less preprocessing time required) and better suited for local interpolation problems compared to Fourier-based techniques.

## 2 CONVOLUTION INTERPOLATION

From the Whittaker-Shannon sampling theorem [11–13] it follows that exact reconstruction of a continuous  $N$ -dimensional ( $ND$ ) image,  $I(\mathbf{x})$ ,  $\mathbf{x} = (x_1, \dots, x_N) \in \mathbb{R}^N$ , from its samples,  $I_s(\mathbf{p})$ ,  $\mathbf{p} = (p_1, \dots, p_N) \in \mathbb{Z}^N$ , is possible in those cases where the sampling frequencies  $F_{s_i}$  satisfied the Nyquist criterion:  $F_{s_i} > 2F_{m_i}$ ,  $\forall i = 1, 2, \dots, N$ , with  $F_{m_i}$  the highest frequency in the  $i$ th dimension of the original image  $I$ . The reconstruction process can be described in terms of convolutions, carried out separately in each dimension:

$$I(\mathbf{x}) = (\dots ((I_s(\mathbf{p}) * h(x_1)) * h(x_2)) * \dots) * h(x_N), \quad (1)$$

where the convolution kernel  $h : \mathbb{R} \rightarrow \mathbb{R}$  is the inverse Fourier transform of a 1D box-filter. This kernel can be derived to be the well-known sinc function:

$$h(x) = \text{sinc}(x) \triangleq \frac{\sin(\pi x)}{\pi x}. \quad (2)$$

Although this function is the theoretically optimal convolution kernel for interpolation of originally band-limited images, it is not the ideal kernel in most practical situations. First of all, since the objects that are being imaged have finite spatial support, the resulting images cannot be strictly band limited, which implies that it is not possible for the sampling frequencies to satisfy the Nyquist criterion. Consequently, it is impossible to retrieve the original images exactly from the resulting samples by means of sinc interpolation. Another problem of sinc interpolation is the fact that, since the sinc function has infinite support, Eq. (1) cannot be computed in practice, except in the case of periodic images [14–16], which are not likely to occur in medical imaging. Furthermore, interpolation by means of a band-limiting convolution kernel may result in Gibbs phenomena, which are very disturbing in images.

For convolution-based interpolation, the only solution to these problems is to choose an alternative convolution kernel. However, in order for any kernel to actually interpolate given samples, it *must* satisfy the following requirements, ultimately satisfied by the sinc function:

$$h(x) = \begin{cases} 1, & \text{if } x = 0, \\ 0, & \text{if } x \in \mathbb{Z}, x \neq 0. \end{cases} \quad (3)$$

In the sequel, kernels satisfying (3) will be referred to as *sinc-approximating kernels*, even though there exist infinitely many kernels that satisfy these requirements but do not necessarily “resemble” the sinc function.

## 3 SINC-APPROXIMATING KERNELS

The sinc-approximating kernels included in the evaluation can be divided into two groups: piecewise polynomial kernels and windowed sinc kernels. Apart from

nearest-neighbor interpolation, which replaces the grey-value at every pixel by that of the nearest pixel after transformation, the convolution kernels of all piecewise polynomial schemes can be written as

$$\psi(x) = \begin{cases} \sum_{i=0}^n a_{ij} |x|^i, & \text{if } j - \xi \leq |x| < j + 1 - \xi, \\ 0, & \text{if } m \leq |x|, \end{cases} \quad (4)$$

where  $n \geq 1$  is the degree of the kernel,  $\xi = 1/2$  for  $n$  even and  $\xi = 0$  for  $n$  odd,  $j = 0, 1, \dots, m + \xi - 1$ , and the parameter  $m$  determines the spatial support of the kernel. In the evaluation, we restricted ourselves to the class of kernels for which  $n$  and  $m$  are related by  $n = 2m - 1$ . This class includes the linear interpolation kernel, all Lagrange central interpolation kernels [17, 18], Dodgson’s quadratic kernel [19], all generalized convolution kernels [20], including cubic convolution [21, 22], and all B-spline kernels [23–26]. Note that the latter kernels require prefiltering of the raw image data.

Windowed sinc kernels are obtained by multiplying the sinc function with a window or apodization function of finite spatial support:

$$h(x) = \omega(x) \text{sinc}(x), \quad (5)$$

with

$$\omega(x) = \begin{cases} w(x), & \text{if } 0 \leq |x| < m, \\ 0, & \text{if } m \leq |x|, \end{cases} \quad (6)$$

where  $\omega : \mathbb{R} \rightarrow \mathbb{R}$  is the window function, and  $w : \mathbb{R} \rightarrow \mathbb{R}$  determines the shape of the window in the interval  $(-m, m)$ , with  $m \in \mathbb{N}$ ,  $m \neq 0$ . In the evaluation, the following windows were included: Bartlett, Blackman, Blackman-Harris (both three- and four-term), Bohman, Cosine, Gaussian, Hamming, Hann, Kaiser, Lanczos, Rectangular, and Welch. For definitions and discussions of the spatial and spectral properties of these window functions, we refer to Harris [27] or Wolberg [28].

## 4 QUANTITATIVE EVALUATION

The medical images used in the evaluation were obtained from 3D brain datasets of different modalities, *viz.*, computed tomography (CT), proton-density weighted (PD-w) magnetic resonance imaging (MRI), T1-weighted (T1-w) MRI, T2-weighted (T2-w) MRI, positron emission tomography (PET), single photon emission computed tomography (SPECT), and 3D rotational angiography (3DRA). Images from 2D cerebral X-ray angiography (XRA) sequences were also included. From every subset (eight in total), five datasets were selected. The five CT datasets were of size  $512 \times 512$  times 28, 28, 29, 30, and 33 voxels, respectively, all with a voxel size of  $0.65 \times 0.65 \times 4.0 \text{ mm}^3$ . The PD-w, T1-w, and T2-w MRI datasets (15 in total) were all of size  $256 \times 256 \times 26$  voxels, with a voxel size of  $1.25 \times 1.25 \times 4.0 \text{ mm}^3$ . The five PET datasets were of size  $128 \times 128 \times 15$  voxels,

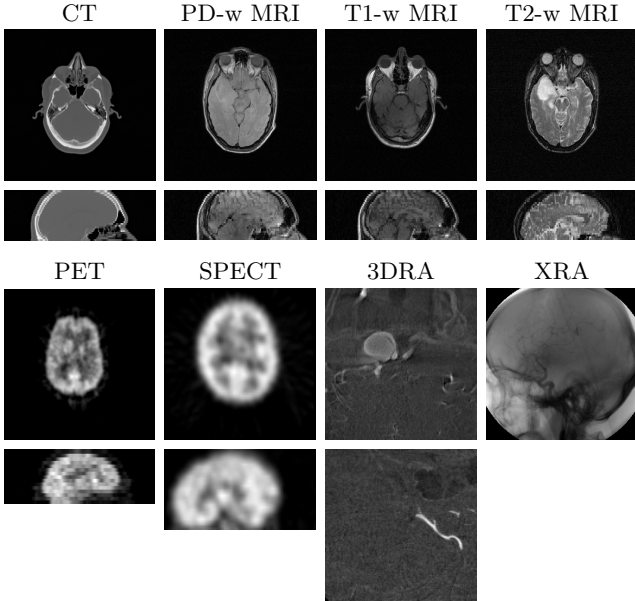


**Figure 1:** Examples of medical test images used in the experiments. For every modality (except XRA, of course), one transversal slice (top image) and one sagittal slice (bottom image) is shown. Note that for display purposes, the images of sagittal slices of the 3D datasets shown in this figure were scaled so as to correct for voxel anisotropy.

one with a voxel size of  $1.94 \times 1.94 \times 8.0 \text{ mm}^3$ , and the others with a voxel size of  $2.59 \times 2.59 \times 8.0 \text{ mm}^3$ . The five SPECT datasets were of size  $64 \times 64$  times 30, 34, 36, 38, and 40 voxels, respectively, all with a voxel size of  $3.91 \times 3.91 \times 3.91 \text{ mm}^3$ . The five 3DRA datasets were all of size  $128 \times 128 \times 128$  voxels, with a voxel size of  $0.6 \times 0.6 \times 0.6 \text{ mm}^3$ . Finally, the five 2D XRA images were all of size  $512 \times 512$  pixels and were arbitrarily selected from their corresponding image sequences. In order to be able to study the performance of the interpolation kernels in different slice directions, one transversal (axial) and one sagittal slice was selected from each of the 3D datasets. This resulted in a total of 75 different 2D test images (see Fig. 1 for examples).

The test images were subjected to rotations and subpixel translations. In the rotation experiments, the 2D test images were successively rotated over  $0.7^\circ$ ,  $3.2^\circ$ ,  $6.5^\circ$ ,  $9.3^\circ$ ,  $12.1^\circ$ ,  $15.2^\circ$ ,  $18.4^\circ$ ,  $21.3^\circ$ ,  $23.7^\circ$ ,  $26.6^\circ$ ,  $29.8^\circ$ ,  $32.9^\circ$ ,  $35.7^\circ$ ,  $38.5^\circ$ ,  $41.8^\circ$ , and  $44.3^\circ$ , which adds up to a total of  $360^\circ$ . These 2D transformations were carried out in the plane of the image. The interpolation errors made in the transversal and sagittal slices are representative for those resulting from a rotation of the entire 3D dataset around its  $z$ - and  $x$ -axis, respectively. In the subpixel translation experiments, the test images were successively shifted over 0.01, 0.04, 0.07, 0.11, 0.15, 0.18, 0.21, 0.24, 0.26, 0.29, 0.32, 0.35, 0.39, 0.43, 0.46, and 0.49 pixels, which adds up to a total of 4.00 pixels. Similar to the rotations, the subpixel translations were

carried out in the plane of the test image. However, these are 1D transformations. For the transversal slices, the translations were carried out in the  $x$ -direction, and for the sagittal slices in the direction corresponding to the through-plane direction in the original 3D dataset. The resulting interpolation errors are representative for those resulting from the application of translations to the entire 3D dataset in these same directions.

For every test image, the experiments were repeated for all interpolation kernels. Of the types mentioned in Section 3, we used all kernels with spatial support equal to or less than 10 sample intervals ( $m \leq 5$ ), which amounts to a total of 126 kernels: the nearest-neighbor and linear interpolation kernel, the quadratic convolution kernel, the cubic, quintic, septic, and nonic convolution kernel using three different values for the free parameter  $\alpha$  [20], the quadratic, cubic, quartic, quintic, sextic, septic, octic, and nonic Lagrange and spline interpolation kernels, and finally 13 families of windowed sinc kernels (of which the Kaiser and Gaussian have a free parameter for which we used four different values), obtained by using five different settings for  $m$ . In order to avoid border problems, all test images were mirrored around the borders in each dimension.

For every combination of test image, experiment (rotation or translation), and interpolation kernel, the cumulative interpolation errors in the resulting processed image were determined. Since in these experiments the grid points of the processed images coincided with those of the corresponding original images, a gold standard was available: for the rotation experiments, the reference images were simply the original images, and for the translation experiments the reference images were obtained by translating the original image by four pixels (which requires no interpolation). The errors were summarized in two FOMs: the root-mean-square error (RMSE) and the largest absolute error (LAE). In order to avoid quantization errors to interfere with the results, all computations were carried out with double precision floating-point numbers (12 significant decimals).

Finally, the relative computational cost of all interpolation kernels was assessed by carrying out a timing experiment, in which a synthetic 3D test image of size  $128 \times 128 \times 128$  voxels was translated over  $(\gamma, \gamma, \gamma)$  voxels (where  $0 < \gamma < 1$  was an arbitrary, but fixed offset) by using non-separated 3D interpolation operations. For this timing experiment, special attention was paid to computationally optimal implementation of each individual interpolation approach.

## 5 RESULTS

In order to get an impression of the performance of the interpolation kernels in terms of the trade-off between accuracy and computational cost, scatter plots were generated. To this end, the five error figures (either RMSEs or LAEs) resulting from every kernel in a given experi-

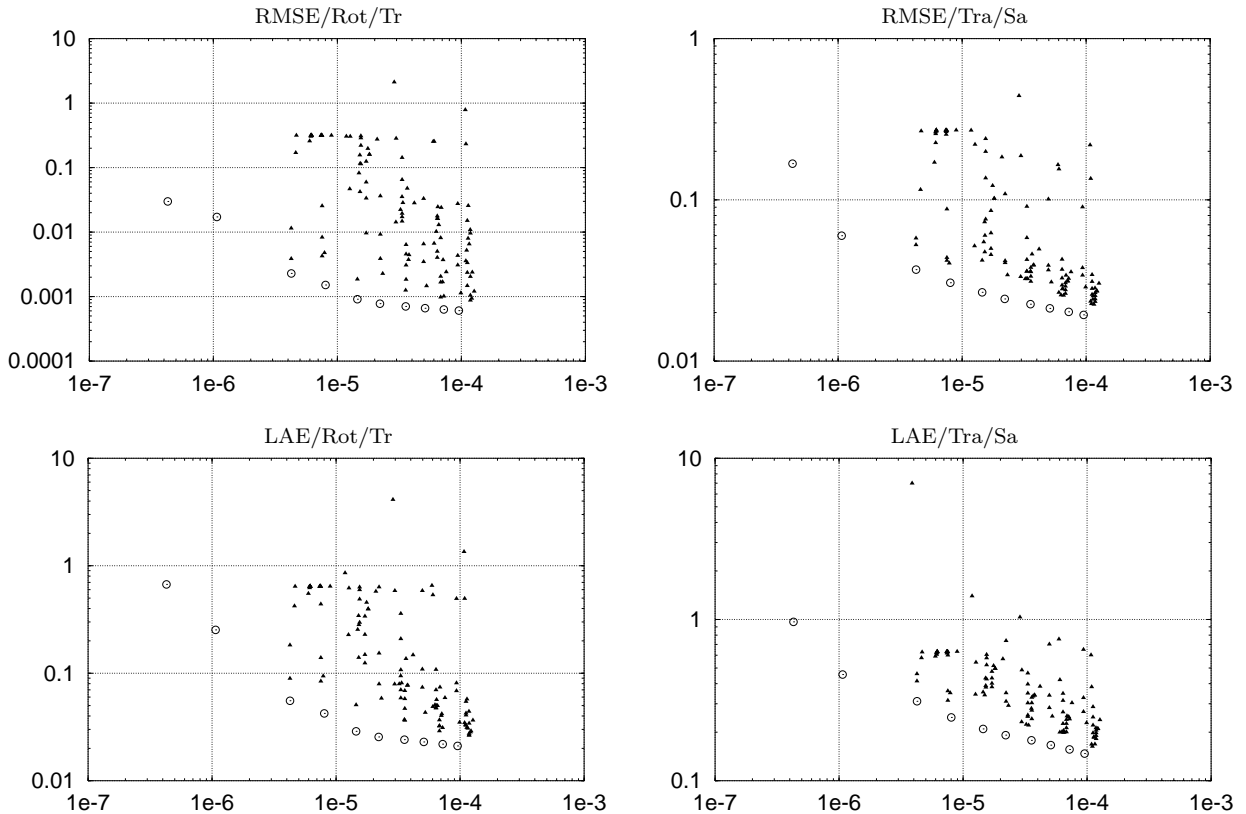


**Figure 2:** Examples of scatter plots showing interpolation error (ordinates) versus computational cost (abscissae) for the different interpolation kernels applied to CT data. The label “A/B/C” on top of each plot provides details concerning the results shown, where A indicates the type of interpolation error (RMSE or LAE), B indicates the type of experiment (rotation (Rot) or translation (Tra)), and C indicates the type of slice (transversal (Tr) or sagittal (Sa)) on which the experiment was carried out. Notice that for every kernel in each plot, the presented FOM is an average of the individual FOMs (expressed as fractions of the dynamic range of grey values) resulting from the five datasets. Also notice that the computational costs (shown here in seconds per voxel) were obtained from separate experiments. Open circles indicate the results of spline interpolation, where the left-most circle corresponds to zeroth-degree and the right-most to ninth-degree spline interpolation.

ment (either rotation or translation) applied to the slices (either transversal or sagittal) of a given group of five datasets from any of the eight different modalities, were averaged. In order to correct for possible intrinsic differences in the dynamic range of grey values between the images within a group of five, the individual error figures were normalized with respect to the dynamic range of their corresponding image, before being averaged.

Regardless of image modality (CT, PD-w MRI, T1-w MRI, T2-w MRI, PET, SPECT, 3DRA, XRA), slice direction (transversal, sagittal), type of experiment (rotation, translation), or figure of merit (RMSE, LAE), spline interpolation was found to yield the best trade-off between accuracy and computational cost: none of the other approaches was more accurate and at the same time computationally cheaper. Scatter plots resulting from several experiments carried out on CT data are shown in Fig. 2. As can be seen, the results of spline interpolation constitute a “lower boundary” in all cases. The same was found for the other modalities.

We note that in the timing experiments, kernel values were determined by exact computations during convolution. In practice, interpolation operations can be accelerated by using look-up tables of densely sampled, precomputed kernel values, with negligible loss of accuracy [28]. With this approach, the relative computational cost of convolution kernels is determined solely by their spatial support. This implies that although spline interpolation seems the best approach in the case of exact computations (Fig. 2), it does not necessarily have to be so when using look-up tables.

In order to compare the accuracy of interpolation approaches for which the corresponding convolution kernels have equal spatial support, the normalized error figures resulting from all kernels in the different experiments were analyzed separately for  $m = 1, 2, 3, 4,$  and  $5$ . For every modality, slice direction, type of experiment, and FOM, the errors figures resulting from spline interpolation in the five images were compared pairwise to the figures resulting from all other meth-

ods with the same spatial support for the corresponding convolution kernel. By using a paired  $t$ -test [29] under the null hypothesis that the methods should yield similar results, the RMSEs resulting from spline interpolation were found to be statistically significantly smaller ( $p < 0.05$ ) in all cases. However, the LAEs resulting from spline interpolation were not always statistically significantly smaller. Especially the Welch, Cosine, Kaiser, and Lanczos windowed sinc kernels performed comparably to higher-degree B-splines in that respect.

## 6 DISCUSSION

A frequently used approach to evaluate interpolation kernels is to compare the spatial and spectral properties of these kernels to those of the sinc function [3, 18, 30–33]. The problem with such approaches is that they are based on the fundamental assumption that in all cases, the sinc function is the optimal interpolation kernel. Apart from that, the conclusions of such evaluations are often not easily translated to specific image processing tasks. Alternatively, interpolation kernels may be compared by subjective visual inspection of image quality, after having used the kernels to perform certain resampling operations [3, 19, 28, 34, 35], or by analyzing their abilities to reconstruct certain mathematical test functions [21]. However, given an image processing task, the most useful evaluation is obtained by applying the kernels to perform that task and then to compare the results to what is considered the gold standard.

In a recently published paper by Grevera & Udupa [6], an elaborate comparison of scene-based and object-based interpolation methods was presented. In the evaluation, 3D medical images were first subsampled in the slice direction with a factor of two. Next, the subsampled images were supersampled with the same factor in order to restore the original dimensions, where the supersampling was carried out by using the different interpolation methods. The resulting images were then compared to their originals. We note that this evaluation approach was designed to assess the performance of interpolation methods for a very specific task: doubling the number of slices for improved 3D object quantification or visualization. The conclusions of this study can not simply be generalized to other interpolation problems, such as the application of geometrical transformations. Moreover, two properties of this evaluation strategy are questionable. First, subsampling introduces additional aliasing artifacts, which interfere with the actual interpolation errors. Because of the low spatial resolution, this is especially true for the slice direction. Second, the evaluation only involves a few distinct samples of the kernels considered. For example, in the evaluation of the cubic convolution kernel, only the values at  $x = -1.5, -0.5, 0.5, 1.5$  are taken into consideration; any arbitrary other function that has the same values at these points would have given the same results.

A frequently used alternative approach to study the performance of interpolation kernels is to apply geometrical transformations to a number of test images, followed by the inverse transformation so as to bring the images back in their original position [2, 4, 5, 20, 33, 36]. This allows for quantitative performance measurements by computing the grey-value differences between the images and their respective originals. However, the negative effects of a kernel in the forward transformation may be canceled out by the backward transformation. In rotation experiments, for example, we have noticed that more than 80% of the errors may be cancelled out in the case of nearest-neighbor interpolation. When using this scheme in a forward-backward subpixel translation operation, the situation is even worse: while we know that this type of interpolation yields very large errors in the forward transformation, the backward transformed image is nevertheless identical to the original image.

In this paper, an alternative evaluation strategy was used. Rather than analyzing the spatial and spectral properties of interpolation kernels compared to the sinc function, we studied the actual performance of these kernels for the specific task of applying geometrical transformations to real medical image data. The strategy is a refined version of an approach used by Unser *et al.* [37], who considered rotation over  $16 \times 22.5^\circ = 360^\circ$ . The approach is entirely objective in the sense that it does not involve artificially created gold standards. It circumvents the aforementioned problems with other approaches: the test images are treated at their intrinsic resolution, thereby avoiding additional aliasing artifacts due to subsampling. Furthermore, by taking into consideration a large number of different rotation angles and translation vectors, interpolation errors are contributed to by the entire shape of the kernels, not just by a limited number of kernel samples. Finally, only forward transformations are applied in order to better avoid cancellation of errors.

The results of the evaluation indicated that spline interpolation is superior compared to all other methods included in this study. An explanation for this superiority may be obtained from approximation theory: it has been shown recently by Blu & Unser [38] that spline interpolation has the largest possible order of approximation, given the spatial support of the B-spline convolution kernel. This implies that, given the samples of any originally continuous input image, the interpolated image resulting from splines converges most rapidly to the original image as the inter-sample distance vanishes. Although there exist other interpolation kernels with this property, such as the Lagrange central interpolation kernels, splines have the unique additional property that they also yield the smoothest interpolant: in contrast with all other approaches considered in this paper,  $n$ th-degree spline interpolation results in an interpolant which is  $n - 1$  times continuously differentiable. We refer to Table 1 for an overview of the convolution kernels

Kernel	Support	Smoothness	Convergence	Notes
Nearest-neighbor	1	–	$\mathcal{O}(\Delta^1)$	
Linear	2	$C^0$	$\mathcal{O}(\Delta^2)$	
Lagrange	$n + 1$	$C^0$	$\mathcal{O}(\Delta^{n+1})$	$n \geq 1$ odd
	$n + 1$	–	$\mathcal{O}(\Delta^{n+1})$	$n \geq 2$ even
Dodgson	3	$C^0$	$\mathcal{O}(\Delta^2)$	
Generalized convolution	$n + 1$	$C^{n-2}$	$\mathcal{O}(\Delta^3)$	$n \geq 3$ odd, $\alpha = \alpha_b$
	$n + 1$	$C^{n-2}$	$\mathcal{O}(\Delta^1)$	$n \geq 3$ odd, $\alpha \neq \alpha_b$
B-spline	$n + 1$	$C^{n-1}$	$\mathcal{O}(\Delta^{n+1})$	requires prefiltering for $n \geq 2$
Bartlett, Blackman-Harris, Hamming windowed sinc	$2m$	$C^0$	$\mathcal{O}(\Delta^0)$	
Gaussian windowed sinc	$2m$	$C^0$	$\mathcal{O}(\Delta^0)$	$\forall \alpha \in \mathbb{R}^+$
Kaiser windowed sinc	$2m$	$C^0$	$\mathcal{O}(\Delta^0)$	$\forall \alpha \in \mathbb{R}^+, \alpha < \infty$
Cosine, Lanczos, Welch windowed sinc	$2m$	$C^1$	$\mathcal{O}(\Delta^0)$	
Blackman, Bohman, Hann windowed sinc	$2m$	$C^2$	$\mathcal{O}(\Delta^0)$	

**Table 1:** The convolution kernels and some of their properties: spatial support, smoothness or regularity, and the rate of convergence of the resulting interpolant. In the second-last column, “ $\mathcal{O}$ ” denotes Landau’s order symbol and  $\Delta$  is the inter-sample distance. Furthermore,  $\alpha_b$  in the last column denotes the value of the free parameter for generalized convolution kernels resulting from the flatness constraint [20].

incorporated in this study and their corresponding properties as mentioned in this paragraph: spatial support, smoothness or regularity, and the rate of convergence of the resulting interpolant.

In order to give an impression of the errors introduced by spline interpolation of different degrees, the results of the rotation experiment for a transversal slice of a T1-weighted MRI dataset, as well as a sagittal slice of a PET dataset, are shown in Figs. 3 and 4, respectively. We note that the errors made in both the rotation and subpixel translation experiments are cumulative errors. That is, they are considerably larger than the errors in practical interpolation problems of the same nature; one usually does not perform *e.g.* rotation by successive intermediate rotations. Nevertheless, the experiments give a representative impression of the average relative performance of the different interpolation kernels.

As can be appreciated from the plots in Fig. 2, the errors in the through-plane direction can be several orders of magnitude larger than those made in the in-plane direction in datasets with a relatively large voxel anisotropy (in the present experiments notably the CT, MRI, and PET datasets). This can be explained from sampling theory: the lower the sampling frequency, the more pre- and post-aliasing artifacts can be expected to be introduced by sampling and interpolation operations. This implies that in order to reduce interpolation

errors when performing fully 3D transformations, it is inefficient to choose a more accurate kernel for the in-plane interpolations, if nothing is done to considerably improve the through-plane interpolations. For instance, for the CT and PET datasets considered in this evaluation, about ninth-degree spline interpolation was required in the through-plane direction in order to have similar RMSEs as linear interpolation in the in-plane direction. For the other modalities, the difference between in-plane and through-plane interpolation errors was less drastic, due to the smaller voxel anisotropy.

Finally, a note concerning the computational cost of spline interpolation. As mentioned in Section 3, and indicated in Table 1, interpolation by means of B-spline convolution kernels requires prefiltering of the raw image data for all degrees  $n \geq 2$ . Although the timing experiments indicated that spline interpolation (including the prefiltering) is computationally cheaper than windowed sinc interpolation, it is somewhat more expensive than the alternative piecewise polynomial schemes. When using look-up tables, the required prefiltering causes spline interpolation to be the computationally most expensive approach. However, since the prefiltering operations can always be carried out separably, their computational cost becomes relatively small in higher-dimensional interpolation problems. Moreover, in applications where many transformations have to be applied to the origi-

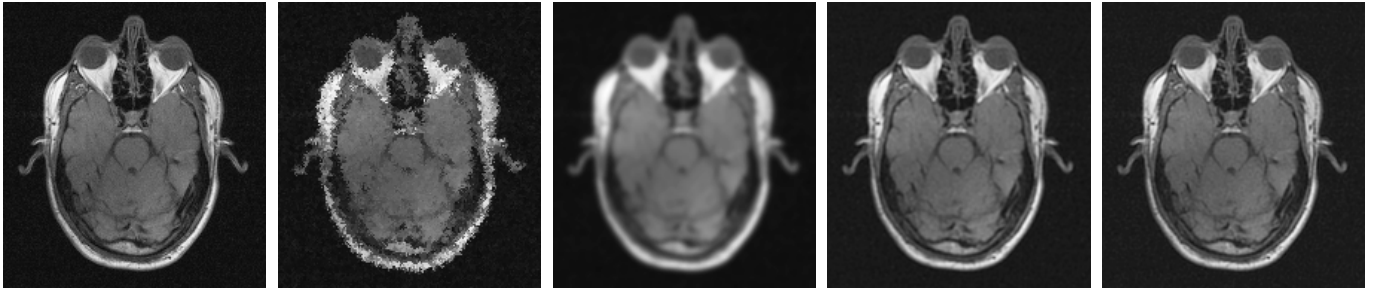


**Figure 3:** Visual impression of the errors resulting from the rotation experiment carried out on a transversal slice of a T1-weighted MRI dataset (left), when using (from second left to right) nearest-neighbor (zeroth-degree spline) interpolation, linear (first-degree spline) interpolation, and cubic and quintic spline interpolation, respectively.



**Figure 4:** Visual impression of the errors resulting from the rotation experiment carried out on a sagittal slice of a PET dataset (left), when using (from second left to right) nearest-neighbor (zeroth-degree spline) interpolation, linear (first-degree spline) interpolation, and cubic and quintic spline interpolation, respectively. Note that the displayed images are scaled so as to visually correct for the voxel anisotropy.

nal image, such as in registration and visualization, the prefiltering needs to be carried out only once, so that the additional cost becomes negligible. Therefore, in the plots shown in Fig. 2, only the computational costs of the actual convolution operations were used.

## 7 CONCLUSIONS

In this paper, a quantitative evaluation of convolution-based methods for medical image interpolation was presented. The evaluation comprised the application of geometrical transformations (rotations and subpixel translations) to medical images from different modalities (CT, MRI, PET, SPECT, 3DRA, and XRA), by using different sinc-approximating kernels. The interpolation errors in the resulting transformed images were analyzed by computing the root-mean-square (RMSE) and the largest absolute (LAE) deviation from the corresponding reference images. The evaluation was designed in such a way that the original images could be used as references. In total, 126 different kernels were evaluated, including piecewise polynomial kernels (nearest-neighbor, linear, Lagrange, generalized convolution, and B-spline) and a large number of windowed sinc kernels (Bartlett, Blackman, Blackman-Harris, Bohman, Cosine, Gaussian, Hamming, Hann, Kaiser, Lanczos, Rectangular, and Welch windows), with spatial supports ranging from 2 to 10 sample intervals.

The combined results of accuracy and timing experiments showed that regardless of image modality, slice direction (transversal or sagittal), type of transformation (rotation or translation), or figure of merit (RMSE

or LAE), spline interpolation constitutes the best trade-off between accuracy and computational cost. That is to say, none of the other approaches included in this study was more accurate and at the same time computationally cheaper. In addition, pairwise comparisons of the error figures resulting from kernels with equal spatial support indicated that spline interpolation is statistically significantly better in the vast majority of cases. Therefore, it is concluded that spline interpolation is to be preferred over all other methods. Cubic spline interpolation resulted in a considerable (28%–91%) reduction of interpolation errors as compared to linear interpolation. Even better results (66%–98% reduction) were obtained with higher-degree spline interpolation, albeit at a considerable increase in computational cost.

## ACKNOWLEDGMENTS

The CT and PET datasets, as well as the PD-, T1-, and T2-weighted MRI datasets were obtained from Vanderbilt University and were originally used in the project “Evaluation of Retrospective Image Registration”, National Institutes of Health, Project Number: 1 R01 NS33926-01, Principal Investigator: Prof. Dr. J. M. Fitzpatrick, Vanderbilt University, Nashville, TN, USA. The SPECT datasets were provided by Prof. Dr. J. K. Buitelaar (University Medical Center Utrecht, the Netherlands) and Dr. R. Stokking (Image Processing and Analysis Group, Yale University School of Medicine). The 3DRA and XRA datasets were made available by Prof. Dr. W. P. Th. M. Mali (University Medical Center Utrecht, the Netherlands) and Philips Medical Systems (Department of X-Ray Diagnostics/Predevelopment, Best, the Netherlands).

## REFERENCES

- [1] J. P. W. Pluim, J. B. A. Maintz, & M. A. Viergever, "Interpolation artefacts in mutual information-based image registration", *Computer Vision and Image Understanding*, vol. 77, no. 2, 2000, pp. 211–232.
- [2] J. V. Hajnal, N. Saeed, E. J. Soar, A. Oatridge, I. R. Young, & G. M. Bydder, "A registration and interpolation procedure for subvoxel matching of serially acquired MR images", *Journal of Computer Assisted Tomography*, vol. 19, no. 2, 1995, pp. 289–296.
- [3] J. A. Parker, R. V. Kenyon, & D. E. Troxel, "Comparison of interpolating methods for image resampling", *IEEE Transactions on Medical Imaging*, vol. 2, no. 1, 1983, pp. 31–39.
- [4] J. L. Ostuni, A. K. S. Santha, V. S. Mattay, D. R. Weinberger, R. L. Levin, & J. A. Frank, "Analysis of interpolation effects in the reslicing of functional MR images", *Journal of Computer Assisted Tomography*, vol. 21, no. 5, 1997, pp. 803–810.
- [5] T. M. Lehmann, C. Gönnér, & K. Spitzer, "Survey: Interpolation methods in medical image processing", *IEEE Transactions on Medical Imaging*, vol. 18, no. 11, 1999, pp. 1049–1075.
- [6] G. J. Grevera & J. K. Udupa, "An objective comparison of 3-D image interpolation methods", *IEEE Transactions on Medical Imaging*, vol. 17, no. 4, 1998, pp. 642–652.
- [7] S. P. Raya & J. K. Udupa, "Shape-based interpolation of multidimensional objects", *IEEE Transactions on Medical Imaging*, vol. 9, no. 1, 1990, pp. 32–42.
- [8] G. J. Grevera & J. K. Udupa, "Shape-based interpolation of multidimensional grey-level images", *IEEE Transactions on Medical Imaging*, vol. 15, no. 6, 1996, pp. 881–892.
- [9] Y. P. Du, D. L. Parker, W. L. Davis, & G. Cao, "Reduction of partial-volume artifacts with zero-filled interpolation in three-dimensional MR angiography", *Journal of Magnetic Resonance Imaging*, vol. 4, no. 5, 1994, pp. 733–741.
- [10] W. F. Eddy, M. Fitzgerald, & D. C. Noll, "Improved image registration by using Fourier interpolation", *Magnetic Resonance in Medicine*, vol. 36, no. 6, 1996, pp. 923–931.
- [11] E. T. Whittaker, "On the functions which are represented by the expansions of interpolation-theory", *Proceedings of the Royal Society of Edinburgh*, vol. 35, 1915, pp. 181–194.
- [12] H. Nyquist, "Certain topics in telegraph transmission theory", *Transactions of the American Institute of Electrical Engineers*, vol. 47, 1928, pp. 617–644.
- [13] C. E. Shannon, "Communication in the presence of noise", *Proceedings of the Institution of Radio Engineers*, vol. 37, no. 1, 1949, pp. 10–21.
- [14] C. Lanczos, *Discourse on Fourier Series*, Oliver & Boyd, London, UK, 1966.
- [15] S. Lanzavecchia & P. L. Bellon, "A moving window Shannon reconstruction algorithm for image interpolation", *Journal of Visual Communication and Image Representation*, vol. 5, no. 3, 1994, pp. 255–264.
- [16] T. Schanze, "Sinc interpolation of discrete periodic signals", *IEEE Transactions on Signal Processing*, vol. 43, no. 6, 1995, pp. 1502–1503.
- [17] R. W. Schafer & L. R. Rabiner, "A digital signal processing approach to interpolation", *Proceedings of the IEEE*, vol. 61, no. 6, 1973, pp. 692–702.
- [18] A. Schaum, "Theory and design of local interpolators", *CVGIP: Graphical Models and Image Processing*, vol. 55, no. 6, 1993, pp. 464–481.
- [19] N. A. Dodgson, "Quadratic interpolation for image resampling", *IEEE Transactions on Image Processing*, vol. 6, no. 9, 1997, pp. 1322–1326.
- [20] E. H. W. Meijering, K. J. Zuiderveld, & M. A. Viergever, "Image reconstruction by convolution with symmetrical piecewise  $n$ th-order polynomial kernels", *IEEE Transactions on Image Processing*, vol. 8, no. 2, 1999, pp. 192–201.
- [21] R. G. Keys, "Cubic convolution interpolation for digital image processing", *IEEE Transactions on Acoustics, Speech, and Signal Processing*, vol. 29, no. 6, 1981, pp. 1153–1160.
- [22] S. K. Park & R. A. Schowengerdt, "Image reconstruction by parametric cubic convolution", *Computer Vision, Graphics and Image Processing*, vol. 23, no. 3, 1983, pp. 258–272.
- [23] M. Unser, A. Aldroubi, & M. Eden, "Fast B-spline transforms for continuous image representation and interpolation", *IEEE Transactions on Pattern Analysis and Machine Intelligence*, vol. 13, no. 3, 1991, pp. 277–285.
- [24] M. Unser, A. Aldroubi, & M. Eden, "B-spline signal processing: Part I — Theory", *IEEE Transactions on Signal Processing*, vol. 41, no. 2, 1993, pp. 821–833.
- [25] M. Unser, A. Aldroubi, & M. Eden, "B-spline signal processing: Part II — Efficient design and applications", *IEEE Transactions on Signal Processing*, vol. 41, no. 2, 1993, pp. 834–848.
- [26] M. Unser, "Splines: A perfect fit for signal and image processing", *IEEE Signal Processing Magazine*, vol. 16, no. 6, 1999, pp. 22–38.
- [27] F. J. Harris, "On the use of windows for harmonic analysis with the discrete Fourier transform", *Proceedings of the IEEE*, vol. 66, no. 1, 1978, pp. 51–83.
- [28] G. Wolberg, *Digital Image Warping*, IEEE Computer Society Press, Washington, USA, 1990.
- [29] D. G. Altman, *Practical Statistics for Medical Research*, Chapman & Hall, London, UK, 1991.
- [30] E. Maeland, "On the comparison of interpolation methods", *IEEE Transactions on Medical Imaging*, vol. 7, no. 3, 1988, pp. 213–217.
- [31] S. K. Park & R. A. Schowengerdt, "Image sampling, reconstruction, and the effect of sample-scene phasing", *Applied Optics*, vol. 21, no. 17, 1982, pp. 3142–3151.
- [32] S. R. Marschner & R. J. Lobb, "An evaluation of reconstruction filters for volume rendering", in *Proceedings of the IEEE Conference on Visualization (Visualization '94)*, R. D. Bergerson & A. E. Kaufman (eds.), IEEE Computer Society Press, Los Alamitos, California, USA, 1994, pp. 100–107.
- [33] R. Machiraju & R. Yagel, "Reconstruction error characterization and control: A sampling theory approach", *IEEE Transactions on Visualization and Computer Graphics*, vol. 2, no. 4, 1996, pp. 364–378.
- [34] H. S. Hou & H. C. Andrews, "Cubic splines for image interpolation and digital filtering", *IEEE Transactions on Acoustics, Speech, and Signal Processing*, vol. 26, no. 6, 1978, pp. 508–517.
- [35] W. F. Schreiber & D. E. Troxel, "Transformation between continuous and discrete representations of images: A perceptual approach", *IEEE Transactions on Pattern Analysis and Machine Intelligence*, vol. 7, no. 2, 1985, pp. 178–186.
- [36] P.-E. Danielsson & M. Hammerin, "High-accuracy rotation of images", *CVGIP: Graphical Models and Image Processing*, vol. 54, no. 4, 1992, pp. 340–344.
- [37] M. Unser, P. Thévenaz, & L. Yaroslavsky, "Convolution-based interpolation for fast, high-quality rotation of images", *IEEE Transactions on Image Processing*, vol. 4, no. 10, 1995, pp. 1371–1381.
- [38] T. Blu & M. Unser, "Quantitative Fourier analysis of approximation techniques: Part I — Interpolators and projectors", *IEEE Transactions on Signal Processing*, vol. 47, no. 10, 1999, pp. 2783–2795.